IEAGHG 8th Post Combustion Capture Conference

16th to 18th September 2025 Marseille, France

Micro-mechanism of CO_2 absorption enhancement in RPBs: Analysis of droplet-wire impact dynamics and mass transfer

Zhenchang Fang[a], Liu Yang[b], Kaijia Jiang[a], Takeshi Hagio[c], Xinqi Qiao[a], Xinling Li[b,d,*], Zhen Huang[b]

[a]*Key Laboratory of Power Machinery and Engineering, Ministry of Education, Shanghai Jiao Tong University, Shanghai 200240, China*
[b]*College of Smart Energy, Shanghai Jiao Tong University, Shanghai 200240, China*
[c]*Institute of Materials Innovation, Institutes of Innovation for Future Society, Nagoya University, Nagoya 464-8601, Japan*
[d]*Institute of Eco-Chongming (IEC), Shanghai 200240, China*

Abstract

Ocean-going cargo ships predominantly powered by diesel play a pivotal role in international trade. However, the CO_2 emissions from their engine exhaust significantly pollute port cities and marine environments [1,2]. In response, the IMO has set a target of achieving net-zero emissions for the shipping industry by around 2050 [3]. Among various ship decarbonization technologies, chemical absorption has garnered considerable attention due to its technical maturity and minimal vessel modification requirements. Nevertheless, traditional packed towers used in chemical absorption face limitations such as large volume, low mass transfer efficiency, and poor adaptability to engine dynamic operating conditions, which severely hinder their large-scale application [4]. Compared with packed towers, rotating packed beds (RPB) enhance gas-liquid contact through centrifugal force, offering advantages including compact design, dynamic adaptability, high mass transfer efficiency, and rapid response flexibility. These characteristics make them more suitable as mass transfer intensification devices for onboard carbon capture systems, with their reliability validated by offshore platform experiments [5].

As shown in Fig. 1(a), the amine solution is ejected outward from the inner layer of the annular rotating packing and dispersed into fine droplets under the shear and tension action of the steel wires. Meanwhile, CO_2 exhaust gas is injected from the outer layer of the wire packing toward the inner layer, enabling highly efficient countercurrent contact between gas and liquid phases within the wire packing. During this process, CO_2 is transferred from the gas to the liquid phase through selective chemical reactions to complete the absorption process. The key to improving mass transfer efficiency is to shear and stretch the amine liquid by the rotating wire packing to increase the gas-liquid contact area. However, the opaque nature of wire packing and the environmental complexity of high turbulence in centrifugal fields seriously hinder the development and optimization of gas-liquid interaction mechanisms.

To reveal the amine droplet breakup dynamics and interfacial mass transfer mechanisms at the microscopic level, this study proposes to deconstruct the complex wire packing as Fig. 1(b) into its fundamental unit - the micro-scale process of a single amine droplet impacting on a steel wire, as shown in Fig. 1(c). A visualization system capable of precisely controlling the CO_2/N_2 atmosphere is developed. High-speed camera technology (8000 fps) is used to capture microsecond-scale droplet breakup processes.

* Corresponding author. Tel.: +86-135-2409-8406
E-mail address: lxl@sjtu.edu.cn

A CFD model with CO_2 absorption chemical reactions is developed to reveal the evolution of concentration fields. This microscale mechanical decoupling method breaks through the "black box" limitations of traditional macroscopic research on the RPBs, enabling precise observation of interfacial liquid breakup and mass transfer. It provides theoretical foundations and design guidelines for the structural optimization of next-generation high-efficiency RPBs.

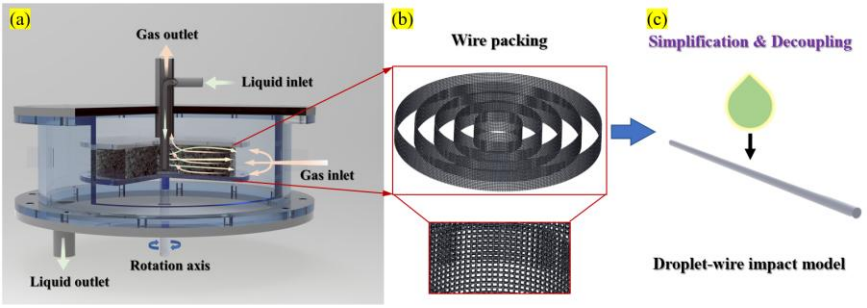

Fig. 1 Decoupling the breakup process of amine solution in wire packing into droplet-wire impact model.

In the RPBs, the continuous absorption of CO_2 by the amine solution alters its viscosity, affecting its motion patterns. Considering the above conditions, this study established the visualization system shown in Fig. 2, which enables precise control of the CO_2/N_2 atmosphere. The system includes a high-speed camera (8000 fps), an LED source, a microfluidic pump with an injector, a transparent acrylic box, and stainless wires of different diameters with optical glass support.

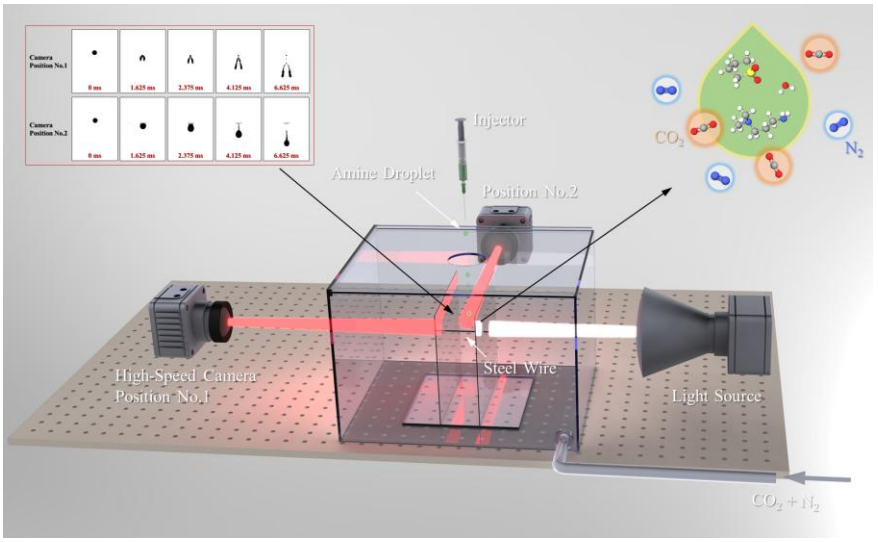

Fig. 2 The drop-wire impact visualization system.

During the experiment, the CO_2/N_2 mixed gas was continuously introduced into the acrylic box at a flow rate of 200 ml/min to maintain a specific CO_2 environment. The microfluidic pump drove the injector to generate droplets of constant size. By adjusting the height, droplets impacted the stainless wire with different initial velocities. This velocity was mapped to the motion parameters of droplets in the centrifugal force field of the RPB, establishing an experimental correspondence among "droplet release height - droplet impact velocity - centrifugal force field effect". The droplet impacting the stainless wire was recorded by the high-speed camera. Changing the position of the high-speed camera allows images to be obtained from both perpendicular and parallel wire views. Different droplets can be obtained by changing the type of needle. The correspondence between droplet size and needle is shown in Fig. 3. In this study, the amine solution was selected as DMAPA-sulfolane-water biphasic absorbent with a high absorption rate and large absorption capacity developed by our group [6]. The concentration of DMAPA was 2 M, and the volume ratio of sulfolane to water was 6:4. As a supplement to the experiment, CFD simulation can obtain detailed information about the CO_2 concentration field. It can help to analyze the connection between the droplet dispersion characteristics and the mass transfer enhancement effect. The CFD geometric model and mesh are shown in Fig. 4.

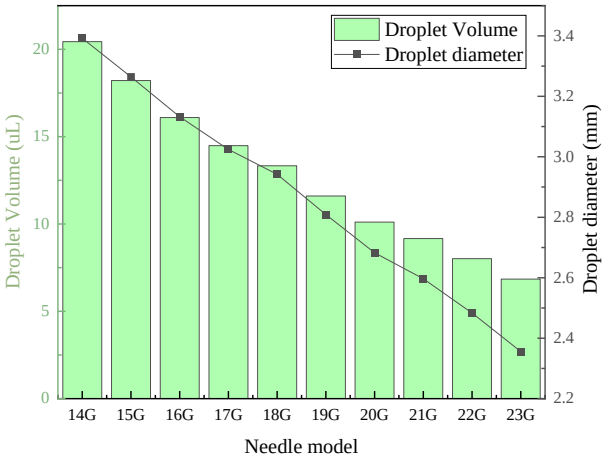

Fig. 3 Correspondence between droplet size and needle type.

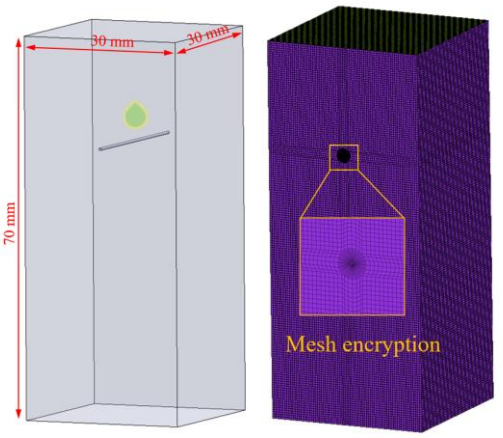

Fig.4 CFD geometric model and mesh.

MATLAB and Image J were used to process the experimental images. As shown in Fig. 5, the image processing steps were: background removal, binarization, and holes filling. The size of the image pixels was calibrated in the experiments using a film ruler with an accuracy of 0.01 mm. Image processing calculates liquid retention, mass transfer area, and droplet stretch length.

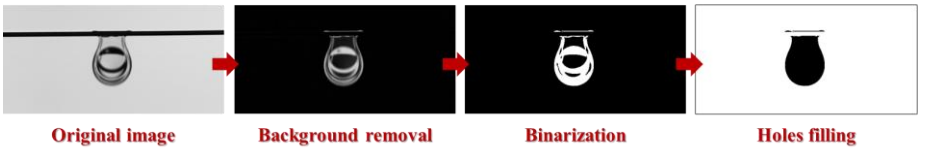

Fig. 5 Droplet image processing diagram.

A 14G needle generated droplets with a diameter of 3.39 mm. Adjusting the release height revealed three typical impact patterns: merge-shaped, λ-shaped, and inverted V-shaped. As shown in Fig. 6(a), when the droplet release height is low, that is, the rotating packed bed speed is low, the droplet pattern is "merge-shaped". The main characteristic is that the droplet splits into two main streams upon impact (1.625 ms), and then the two streams merge during the secondary expansion process (7.000 ms). Due to surface tension, the merged droplets are connected to the stainless wire by an elongated liquid line as they fall (11.750 ms). Over time, the elongated liquid line breaks into several fine droplets due to inertia, surface tension, and local pressure (12.375-14.875 ms), and the fine droplets randomly collide and merge (18.375 ms). Finally, the large droplets with followed fine droplets fall in the direction of gravity (31.625 ms).

The λ-shape is shown in Fig. 6(b)-(c). At the initial stage of the droplet impacting the stainless wire, the λ-shaped is similar to the merge-shaped, except that the two streams of the λ-shaped are stretched longer under the gravitational potential energy (fig. 6(c) 4.125 ms). Meanwhile, the λ-shaped also suffers from the secondary expansion effect, but the two streams are implicated only at the tail (fig. 6(c) 4.875 ms). Then, the liquid line connecting the droplet with the stainless wire continues to extend, and together with the two streams, it takes on a "λ" shape (fig. 6(c) 6.250 ms). With the breakage of the liquid line, the two streams gradually separated and fell in the direction of gravity.

The initial difference between inverted V-shaped, merge-shaped, and λ-shaped is mainly reflected in the droplet stretching length, as shown in Fig. 6(d). With the increase of the stretching length, the two streams show fine necking at the tail, which leads to the shrinkage of the secondary expansion area, and the two streams show a discrete state (3.875 ms) after the secondary expansion. In addition, the duration of the liquid line in the inverted V-shape showed a significant height dependence: when the release height was increased from 50 mm to 300 mm, its duration decreased sharply from 5.375 ms to 0.625 ms (-88.4%). High-speed images show that the two streams and their accompanying liquid lines together form an inverted V-shape (4.125 ms). Typical characteristics of this shape also include the formation of an elongated trailing structure on the droplets after the liquid lines break, which goes through the phenomena of contraction, breakage, and fusion sequentially during the droplets falling (8.875 - 12.000 ms). Kinetic analyses show that the increase in release height causes the droplet kinetic energy to dominate, thus breaking the constraints imposed by surface tension and local pressure gradient on the droplet shape.

From merge-shaped, λ-shaped to inverted V-shaped, corresponding to the low, medium, and high-speed of the RPBs respectively, with large differences in contact area and maintenance time. Although the total contact area is larger for the inverted V-shape, the maintenance time for the merge-shaped and λ-shape is 19.625 ms and 9.125 ms, respectively, larger than that for the

inverted V-shape. Considering that the chemical reaction rate depends on the reaction time and contact area, the increased maintenance time may compensate for the lack of contact area.

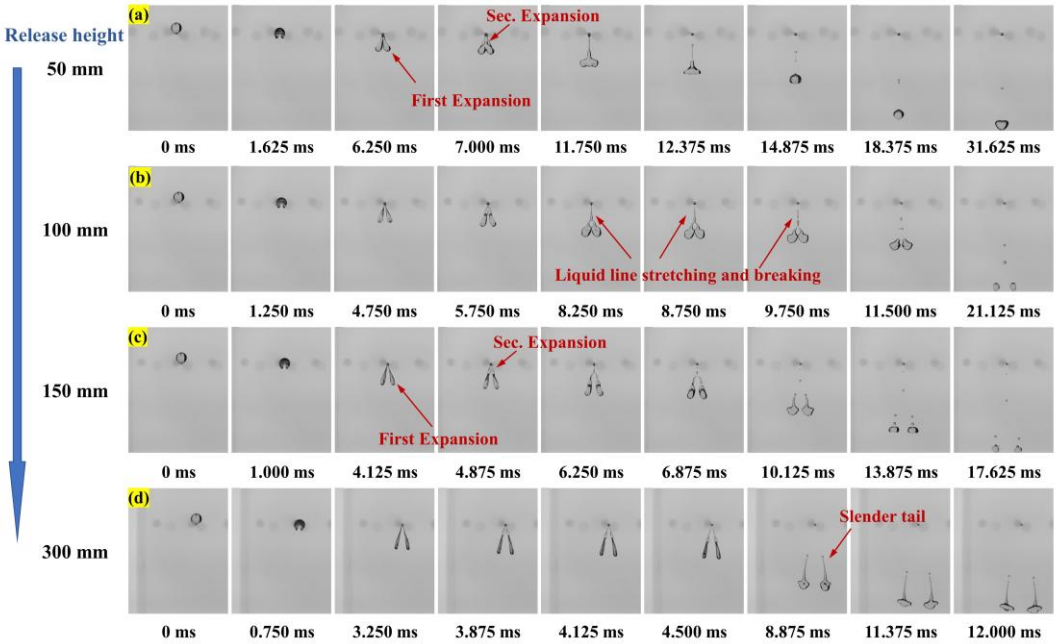

Fig. 6 Patterns after droplet impact the stainless wire.

References

[1] K. Jiang, L. Yang, Z. Fang, N. Ma, X. Li, Z. Huang, Navigating towards a zero-carbon world: Research progress of chemical solvent-based shipboard carbon capture system integration and renewable energy coupling, Ocean Eng. 309 (2024) 118585. https://doi.org/10.1016/J.OCEANENG.2024.118585.

[2] T. Zhao, R. Li, Z. Zhang, C. Song, Current status of onboard carbon capture and storage (OCCS) system: A survey of technical assessment, Carbon Capture Sci. Technol. 15 (2025) 100402. https://doi.org/10.1016/J.CCST.2025.100402.

[3] E.A. Bouman, E. Lindstad, A.I. Rialland, A.H. Strømman, State-of-the-art technologies, measures, and potential for reducing GHG emissions from shipping – A review, Transp. Res. Part D Transp. Environ. 52 (2017) 408–421. https://doi.org/10.1016/J.TRD.2017.03.022.

[4] M. Akram, A. Gheit, K. Milkowski, W. Gale, M. Pourkashanian, Comparison of conventional and process intensified next generation RPB absorbers for decarbonisation of the steel industry, Fuel. 388 (2025) 134484. https://doi.org/10.1016/J.FUEL.2025.134484.

[5] W.C. Chen, W.H. Meng, Z.H. Liu, G.W. Chu, L.L. Zhang, J.F. Chen, Hydrodynamics of gas flow in a rotating packed bed under floating motions: Experimental and simulation study, Chem. Eng. J. 442 (2022) 136149. https://doi.org/10.1016/J.CEJ.2022.136149.

[6] L. Yang, J. Chen, N. Ma, Z. Fang, X. Li, Z. Huang, Novel diamine DMAPA-sulfolane-water biphasic absorbent for equimolar CO2 absorption: Performance and mechanisms, Chem. Eng. J. 479 (2024) 147903. https://doi.org/10.1016/J.CEJ.2023.147903.

Keywords: Onboard carbon capture; Rotating packed bed; Mass transfer enhancement; Biphasic absorbent; High speed camera technology.